IEEE Sensors Council

The Electrical Characteristics of the Co/Giemsa/*n*-Si Heterostructure Depending on Measurement Temperatures and Frequencies

Adem Kocyigit, Sakir Aydogan, Ümit Incekara, and Mehmet Yılmaz

***Abstract*—Giemsa dye was used as an interlayer film structure between Co metal and n-type silicon to fabricate Co/giemsa/*n*-Si heterostructure to determine various electrical behaviors. For that reason, temperature-dependent current voltage (*I*–*V*) and frequency-dependent capacitance voltage (*C*–*V*) measurements were employed to reveal electrical properties of the Co/giemsa/*n*-Si heterostructure for wide range temperature and frequency. Various junction parameters such as series resistance, barrier height, and ideality factor values were determined from *I*–*V* characteristics by thermionic emission (TE), Cheung, and Norde methods. The results revealed that the junction parameters were strong function of the measurement temperature. Frequency dependent *C*–*V* characteristics were also utilized for extraction of various electrical parameters such as maximum electric field, depletion width, barrier height, etc. The results highlighted that all electrical parameters changed as function of the frequency and voltage. The Co/giemsa/*n*-Si heterostructure can be improved for thermal sensing and switching applications.**

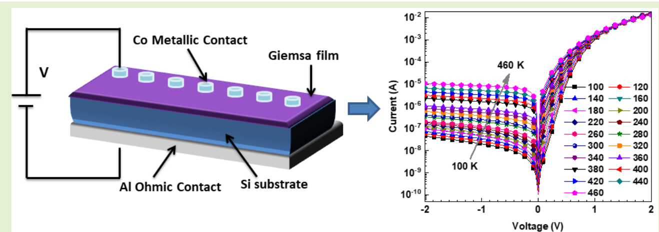

***Index Terms*—Electrical characterization, frequency dependent *C*–*V* characteristics, giemsa, temperature-dependent *I*–*V* characteristics, thermal sensitivity.**

I. Introduction

SEMICONDUCTOR materials are important for electronic and control applications because of their easy adjustability behavior of conductivity [1], [2]. The semiconductors can be employed as substrate materials for various devices or used for fabricating heterostructures with insulator, semiconductor, or metals [3], [4], [5]. When they contact to the metal, either ohmic or metallic contact behaviors occur depending on the work function of the metal and semiconductor in the case of lacking of interface states [6]. The performance and applicability of the device changes depend on the interface in the contact formed between a metal and a semiconductor [7]. Thus, the interface of the contact should be controlled very carefully. The insulator or metal oxide interfacial layers between the metal and the semiconductor are used sometimes to control electrical behaviors of the metal semiconductor heterostructure, and various polymer or insulating materials such as pentacene, chitosan, hematoxylin, aniline blue, or congo red have been successfully used for that reason [8], [9], [10]. Dye-based organic materials are much more advantageous in optical, electrical, and thermal applications compared to inorganic materials in terms of low cost, easy preparation, and use in flexible electronics [11]. Giemsa is a mixture of methylene blue, Azure B, and eosin dyes that stand out with their interesting electrical and optical properties [12], [13], [14], [15], [16], [17]. It also can be employed as interlayer for metal semiconductor heterostructures to control electrical behaviors because it has good photothermal stability and strong optical absorption in the ultraviolet (UV)-Visible region [18].

The characterization of the metal-semiconductor heterostructures can be made by *I*–*V* and *C*–*V* measurements depending on the light power intensity, measurement temperature, or frequency to investigate their electrical behaviors and to reveal their various applications [19], [20], [21]. While the temperature-dependent *I*–*V* characteristics provide to understand electrical conduction mechanism, frequency-dependent *C*–*V* characteristics help to discover dielectric behaviors [22], [23], [24], [25].

Manuscript received 25 December 2022; accepted 6 March 2023. Date of publication 14 March 2023; date of current version 14 April 2023. The associate editor coordinating the review of this article and approving it for publication was Prof. Pai-Yen Chen. *(Corresponding author: Adem Kocyigit.)*

Adem Kocyigit is with the Department of Electronics and Automation, Vocational High School, Bilecik Seyh Edebali University, Bilecik 11000, Turkey (e-mail: adem.kocyigit@bilecik.edu.tr).

Sakir Aydogan is with the Department of Physics, Ataturk University, Erzurum 25240, Turkey (e-mail: saydogan@atauni.edu.tr).

Ümit Incekara is with the Department of Biology, Ataturk University, Erzurum 25240, Turkey (e-mail: uincekara@atauni.edu.tr).

Mehmet Yılmaz, is with the Department of Science Teaching, Ataturk University, Erzurum 25240, Turkey (e-mail: mehmetyilmaz@atauni.edu.tr).

Digital Object Identifier 10.1109/JSEN.2023.3255180

1558-1748 © 2023 IEEE. Personal use is permitted, but republication/redistribution requires IEEE permission.
See https://www.ieee.org/publications/rights/index.html for more information.

Authorized licensed use limited to: Bilecik Seyh Edebali Universitesi. Downloaded on December 11,2025 at 08:33:02 UTC from IEEE Xplore. Restrictions apply.

According to our best knowledge, there is not any application of the giemsa in the metal semiconductor heterostructures in the literature. In this article, giemsa was used as interfacial layer between Co and n-Si, and Co/giemsa/n-Si heterostructure was characterized by I–V and C–V measurements depending on temperature and frequency to find out electrical properties for thermal sensing applications.

II. Materials and Methods

Giemsa was purchased and used directly without purification procedure to obtain giemsa film layer between the Co and n-Si. Giemsa was dissolved in water by stirring for 1 h at 80 °C temperature. Meanwhile, a commercially purchased one-side polished n-type silicon wafer with (100) crystal orientation was sliced to 2×1 cm^2 pieces and cleaned in acetone, isopropanol, and distilled water by an ultrasonic cleaner for 30 min. Furthermore, HF:H_2O (1:10) mix solution were employed to remove natural oxide layers on the pieces in a 30 s. Then, the wafer pieces were put into thermal evaporator to obtain a 100 nm thick Al back contact on the unpolished surfaces of the pieces at 5×10^{-6} torr pressure. The pieces were then annealed for 5 min to achieve ohmic contact in a nitrogen filled oven at 450 °C temperature. The giemsa solution was dropped onto polished surfaces of the pieces and spined at 3000 rpm for 30 s by a spin coater. The pieces were transferred again into thermal evaporator to acquire metallic or Schottky contact on the giemsa layer by a hole array mask which have 7.85×10^{-3} cm^2 hole areas. Thus, Co/giemsa/n-Si heterostructure was fabricated.

Keithley 487 Picoammeter/Voltage Source meter was used to collect I–V data of the Co/giemsa/n-Si heterostructure in a temperature-controlled cryostat system in a temperature range of 100 and 460 K with 20 K steps. Frequency-dependent C–V measurements were obtained by HP 4192A LF impedance analyzer system for the frequency of 100 kHz, 200 kHz, 500 kHz, 1 MHz, 2 MHz, and 3 MHz.

III. Results and Discussion

The ln$I$–V plots of the Co/giemsa/n-Si heterostructure have been shown in Fig. 1(a) for changing temperature from 100 to 460 K. While the forward bias current did not change so much by increasing temperature, reverse bias current increased almost periodically up to 100 folds. The Co/giemsa/n-Si heterostructure can be thought as thermal sensor at reverse biases due to increasing current as a result of increasing temperature [26], [27]. The heterostructure also exhibited good rectifying behavior which is important for stopping reverse current. The rectification ratio (RR) values were calculated for ±1.5 V and listed in Table I. The changes of the RR values have been given in Fig. 1(b) depending on the increasing temperature. The RR values decreased exponentially and almost reached constant value after 360 K temperature. The Co/giemsa/n-Si heterostructure has high RR values even if beyond 360 K temperature. In addition, giemsa has a positive effect on the interface, as can be seen from the I–V measurements at room temperature of devices with and without interfaces (in Fig. 1(b) inset). For example, while the ideality factor was 1.98 at 300 K for the device with giemsa,

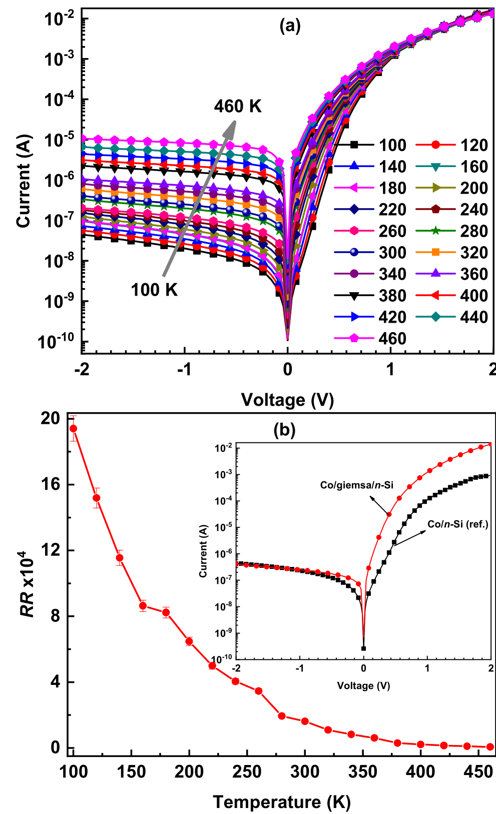

Fig. 1. (a) ln I–V plots of the Co/giemsa/n-Si heterostructure for various temperatures and (b) changing RR values by increasing temperature, and inset figure shows comparison of Co/giemsa/n-Si with Co/n-Si (ref.) in terms of I–V characteristics.

it was calculated as 3.08 for the device without giemsa. This can be explained by the passivation at the interface or the restructuring of the interface states [28], [29].

The threshold voltage is important for heterostructures to turn on the current through the device, and low threshold voltage values are desired [30]. The threshold voltage changes of the Co/giemsa/n-Si heterostructure depending on the measurement temperature have been shown in Fig. 2(a). The threshold voltage values decreased almost linearly by increasing temperature like ref. [31]. This result confirmed that the heterostructure have linear response to the temperature changes and can be used thermal sensing applications. I–V characteristics of the Co/giemsa/n-Si heterostructure were used to determine various parameters such as barrier height (Φ_b), ideality factor (n), and series resistance values (R_s) by thermionic emission (TE) theory, Norde, and Cheung methods. According to TE theory, while the n values decrease by increasing temperature, the Φ_b values increase. The calculation formulas of the n and Φ_b according to TE theory can be found in the literature [32], [33]. Fig. 2(b) indicates barrier height and ideality factor changes of the Co/giemsa/n-Si heterostructure by changing temperature. Whereas the Φ_b values increased linearly, the n values decreased almost exponentially due to non-linear changes of $dV/d\ln I$. Furthermore, saturation current (I_o) of the Co/giemsa/n-Si heterostructure has increased by increasing measurement temperature. The n, Φ_b, and I_o values have been given in Table I depending on the increasing temperature.

Authorized licensed use limited to: Bilecik Seyh Edebali Universitesi. Downloaded on December 11,2025 at 08:33:02 UTC from IEEE Xplore. Restrictions apply.

TABLE I
CALCULATED DEVICE PARAMETERS OF THE CO/GIEMSA/n-SI DEVICE FOR THE TE THEORY, CHEUNG, AND NORDE METHODS

T(K)	I_0 Saturation Current (A)	n (TE)	n (Cheung)	Φ_b (TE) (eV)	Φ_b(Cheung) (eV)	Φ_b(Norde) (eV)	R_s (Cheung) (dv/dlnI-I) (kΩ)	R_s (Cheung) (H(I)-I)) (kΩ)	R_s (Norde) (F(V)-V) (kΩ)	RR
100	7.79×10^{-10}	5.87	5.82	0.26	0.26	0.31	2.08	2.15	3.39	1.94×10^{5}
120	9.10×10^{-10}	4.74	4.87	0.31	0.31	0.37	1.99	2.02	3.38	1.52×10^{5}
140	1.46×10^{-9}	3.95	4.04	0.36	0.36	0.41	1.84	1.78	3.12	1.16×10^{5}
160	2.47×10^{-9}	3.39	3.58	0.41	0.40	0.47	1.72	1.61	3.06	8.64×10^{4}
180	2.38×10^{-9}	2.95	2.95	0.47	0.47	0.52	1.53	1.59	2.91	8.23×10^{4}
200	4.79×10^{-9}	2.62	2.74	0.51	0.51	0.55	1.34	1.35	2.90	6.47×10^{4}
220	9.17×10^{-9}	2.36	2.49	0.55	0.56	0.59	1.33	1.33	2.81	4.99×10^{4}
240	1.21×10^{-8}	2.19	2.36	0.60	0.61	0.64	1.25	1.27	2.76	4.05×10^{4}
260	2.00×10^{-8}	2.16	2.24	0.64	0.65	0.69	1.27	1.26	2.70	3.46×10^{4}
280	4.23×10^{-8}	2.09	2.20	0.68	0.68	0.72	1.43	1.48	2.65	1.94×10^{4}
300	5.63×10^{-8}	1.98	2.08	0.72	0.73	0.75	1.32	1.34	2.60	1.62×10^{4}
320	9.87×10^{-8}	1.94	1.97	0.76	0.77	0.79	1.31	1.33	2.53	1.10×10^{4}
340	1.35×10^{-7}	1.88	1.89	0.80	0.81	0.83	1.20	1.24	2.34	8.20×10^{3}
360	1.78×10^{-7}	1.83	1.82	0.84	0.85	0.86	1.12	1.22	2.05	6.10×10^{3}
380	3.77×10^{-7}	1.82	1.79	0.87	0.88	0.89	1.03	1.05	1.98	2.94×10^{3}
400	5.10×10^{-7}	1.76	1.72	0.91	0.92	0.92	0.92	0.93	1.30	2.12×10^{3}
420	6.82×10^{-7}	1.72	1.66	0.95	0.95	0.98	0.87	0.88	1.16	1.50×10^{3}
440	1.03×10^{-6}	1.69	1.63	0.98	0.99	1.01	0.83	0.84	1.03	1.01×10^{3}
460	1.37×10^{-6}	1.68	1.61	1.02	1.02	1.04	0.79	0.78	0.88	6.36×10^{2}

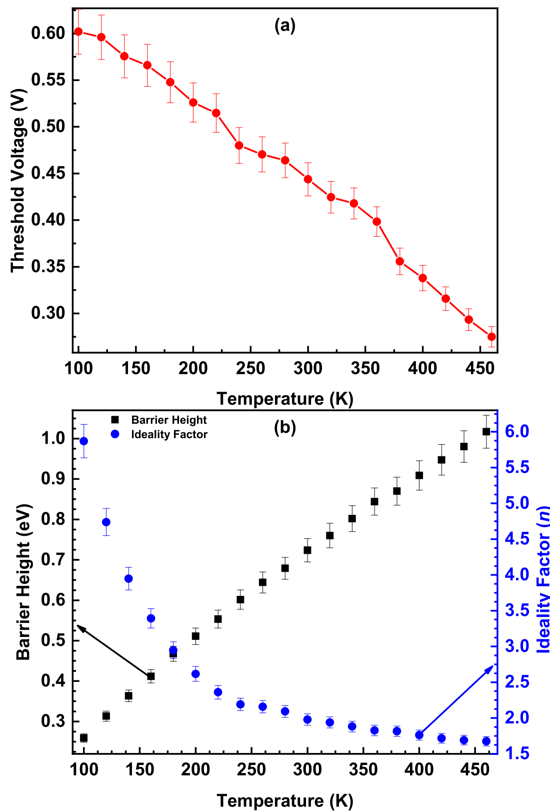

Fig. 2. (a) Changing of the threshold voltage and (b) variation of the n and Φ_b values of the Co/giemsa/n-Si heterostructure depending on the measurement temperature.

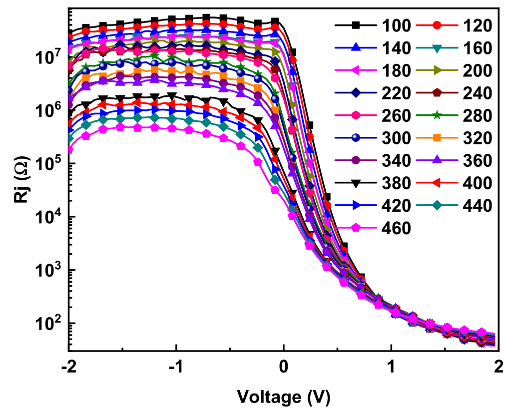

Fig. 3. R_j–V plots of the Co/giemsa/n-Si heterostructure by changing temperature.

Junction resistance (R_j) describes heterostructure of whole resistance. The R_j can be obtained by formula of $R_j = dV/dI$ from I–V measurements [34]. While the reverse bias region represents shunt resistance (R_{sh}), forward bias region resistance shows series resistance (R_s) in the R_j–V plots. While the R_{sh} is related to contact-semiconductor interface, R_s provides information about interfacial layer resistance [35]. Fig. 3 displays R_j versus voltage plots of the Co/giemsa/n-Si heterostructure for changing measurement temperature. The R_j values decreased with increasing temperature almost periodically due to increasing current especially at reverse biases. This result is important for a kind of thermal sensing application. The levels of R_{sh} and R_s values are 10^7 and 10^2 Ω, and these levels are good for an electronic device [36].

When plotting the $n\mathrm{k}T$ versus $\mathrm{k}T$, where k is Boltzmannn constant, current transport mechanism of the heterostructure can be understood. Fig. 4(a) exhibits $n\mathrm{k}T$–$\mathrm{k}T$ plot of the Co/giemsa/n-Si heterostructure. There can be seen two different mechanisms in the $n\mathrm{k}T$–$\mathrm{k}T$ plot: one has negative slope (−0.56) and shows field emission mechanism, another has positive slope (1.06) and represents TE mechanism [37]. Finally, heterostructure has not have pure TE conduction mechanism according to $n\mathrm{k}T$–$\mathrm{k}T$ plot. This effect may be attributed to structure of interfacial giemsa layer.

The Richardson constant calculation can help to determine barrier height and to measure of the barrier inhomogeneities

Authorized licensed use limited to: Bilecik Seyh Edebali Universitesi. Downloaded on December 11,2025 at 08:33:02 UTC from IEEE Xplore. Restrictions apply.

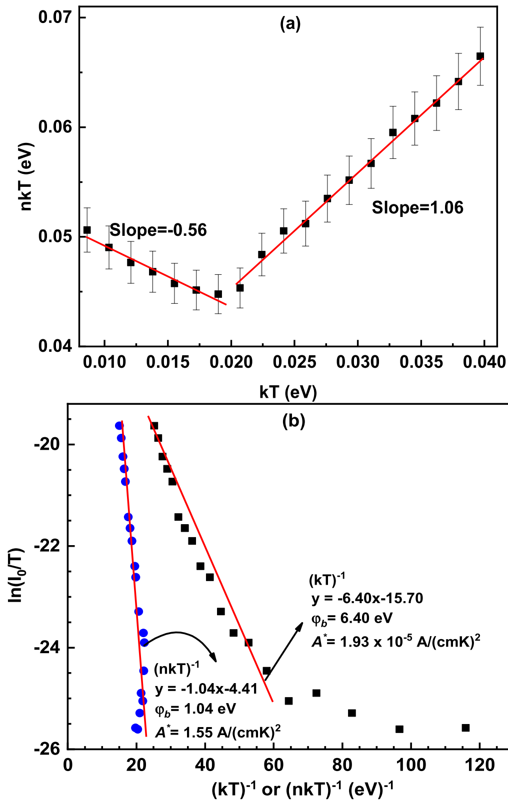

Fig. 4. (a) nkT–kT graphs and (b) experimental Richardson plots of the Co/giemsa/n-Si heterostructure.

of the metal semiconductor heterostructures. The Richardson constant value is usually obtained lower than real value due to barrier inhomogeneity [38]. Fig. 4(b) shows Richardson plots of the Co/giemsa/n-Si heterostructure. The determined barrier height and Richardson constant values are 1.04 eV and 1.55 $Acm^{-2}K^{-2}$, respectively. While the barrier height value is close to its calculated value from other techniques, the Richardson constant value is far from its real value due to barrier inhomogeneities in the heterostructure.

Cheung method can be performed on the I–V characteristics to confirm the accuracy of the ideality factor, barrier height and series resistance values from TE theory, and small deviations can be acceptable due to approximation differences or nonideal junction structure [39]. The Cheung method calculates $dV/d(\ln I)$ and $H(I)$ functions and finds above parameters. Related formulas about Cheung functions and parameter calculation techniques have been found in the literature [40].

The $dV/d(\ln I)$ and $H(I)$ versus current graphs exhibit almost linear lines, and the R_s, Φ_b, and n can be calculated by y-intercepts and slopes of these plots (Not shown here). The calculated Φ_b, n, and R_s values have been listed in Table I for an increasing measurement temperature. The obtained n and Φ_b values are good agreement with the n and Φ_b values from TE method. Furthermore, the R_s values are good harmony each other for $dV/d(\ln I)$ and $H(I)$ which shows the consistency of the Cheung method [41].

Alternatively, Norde method can help to calculate the Φ_b and R_s values by plotting of the Norde function ($F(v)$). The

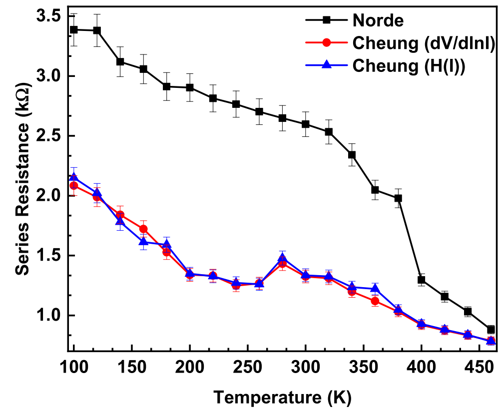

Fig. 5. Changing of the R_S values of the Co/giemsa/n-Si heterostructure depending on the measurement temperature for various calculation techniques.

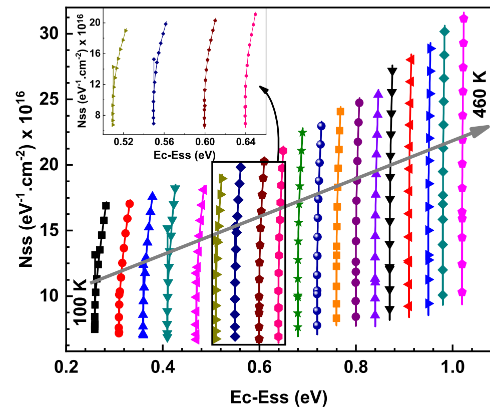

Fig. 6. N_{SS} versus E_C–E_{SS} plots of the Co/giemsa/n-Si heterostructure for various temperatures.

calculation of the Φ_b and R_s values with Norde function can be found everywhere [42], [43]. When the $F(v)$ function is plotted against to voltage, minimum $F(v)$ and related minimum voltage values are used to calculate the Φ_b and R_s values (Not shown here). The calculated Φ_b and R_s values have been tabulated in Table I. Both the Φ_b and R_s values are a little bit higher than that of TE and Cheung's Φ_b and R_s values due to approximation differences [6].

Fig. 5 displays R_s versus temperature plots of the Co/giemsa/n-Si heterostructure for the Norde and Cheung functions. The R_s values of both the Norde and Cheung functions have same decreasing profile for increasing temperature, but R_s values of the Norde a little bit higher than Cheung function's R_s values because of approximation to the I–V characteristics [44], [45].

Another important parameter about the metal semiconductor heterostructure is interface states density (N_{ss}). The temperature dependent N_{ss} profiles should be worked to understand the reaction of the Co/giemsa/n-Si heterostructure depending on the conduction band (E_c) and surface states (E_{ss}) energy levels. Fig. 6 shows N_{ss} versus E_c–E_{ss} plots of the Co/giemsa/n-Si heterostructure for an increasing temperature. The N_{ss} values almost did not changed so much with E_c–E_{ss} values for every temperature condition. However, they increased with increasing temperature in the same E_c–E_{ss} value.

Authorized licensed use limited to: Bilecik Seyh Edebali Universitesi. Downloaded on December 11,2025 at 08:33:02 UTC from IEEE Xplore. Restrictions apply.

TABLE II
COMPARISON OF THE THERMAL SENSITIVITY FOR VARIOUS HETEROJUNCTION DEVICES

Device	Sensitivity values/ranges	Ref.
Co/giemsa/n-Si	-(0.79-1.00) mV/K	**This work**
GO:Fe_3O_4/p-Si	-(1.18-1.05) mV/K	[46]
p-NiO/n-GaN	-(0.61-2.58) mV/K	[47]
4H-SiC	-(0.86-1.18) mV/K	[48]
MOSFET ZTC	-1.45 mV/ ºC	[49]
Lateral GaN	-1.13 mV/K	[50]
GaN/SiC	~(-1) mV/K	[51]
GaAs	-(1.31-3.42) mV/K	[26]
Al_2O_3-Based a-IGZO	-(0.81-1.59) mV/ K	[52]
GaN	~(-1) mV/K	[53]
4H-SiC	-(1.3-2.8) mV/ K	[54]
Diamond	-1.6 mV/K	[55]

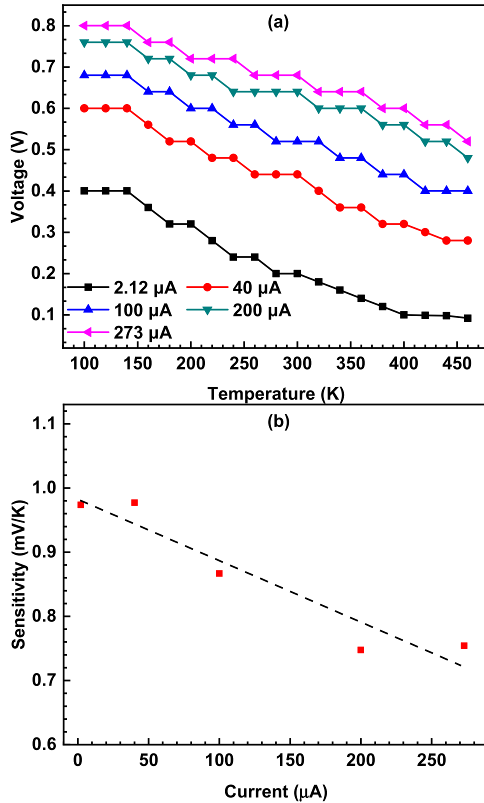

Fig. 7. (a) V–T curves for different forward bias, and (b) sensitivity-current curve for Co/giemsa/n-Si device.

The comparison of the thermal sensitivity for different heterojunction devices is given in Table II. The sensitivity (S) of a thermal device is given in dV/dT. The voltage-temperature graphs of the Co/giemsa/n-Si device for different current values are given in Fig. 7(a). It is clearly seen that the V–T changes are linear for the values considered. In addition, it was observed that the slope decreased with increasing current. S values ranged from ~1 (2.12 μA) to 0.79 mV/K (273 μA), respectively. In addition, the sensitivity-current graph is shown in Fig. 7(b). It is seen that the S value decreases with increasing current.

We also calculated temperature coefficient for Co/giemsa/n-Si device using both reverse bias and forward bias temperature values and using the relation of $R = R_{\text{ref}}\,[1+\alpha(T - T_{\text{ref}})]$.

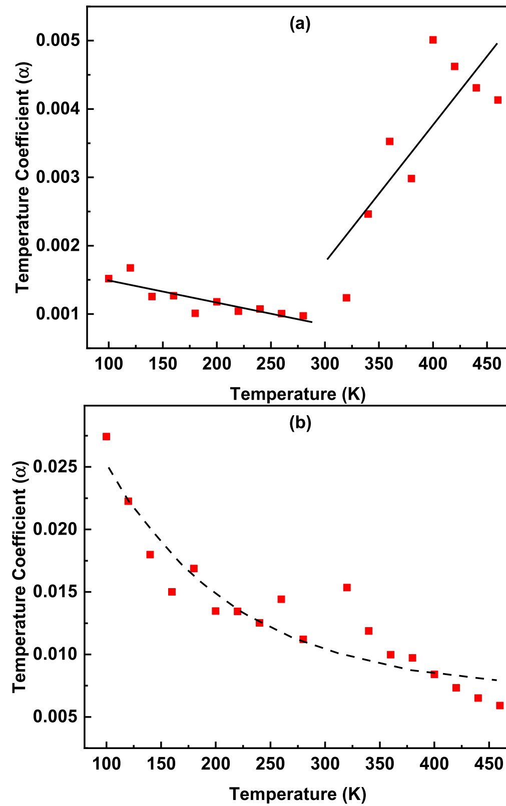

Fig. 8. Temperature coefficient changes of the Co/giemsa/n-Si device depending on measurement temperature. (a) For forward bias resistances. (b) Reverse bias resistances.

Fig. 8(a) and (b) reveal temperature coefficient (α) versus temperature graphs of the Co/giemsa/n-Si device for forward and reverse bias resistance values, respectively. α values decreased linearly toward 300 K temperature, but then increased higher temperatures for forward bias resistances. However, α values decreased almost exponentially from 100 to 460 K temperature for reverse bias resistances. For low temperature and forward biases, α values decreased linearly and can be modeled for a device. However, the higher temperature than room temperature, the α values have many discrepancies. The α values calculated from reverse bias resistances also can be modeled easily. The device can be used and improved for temperature sensing applications.

The capacitance behavior of Co/giemsa/n-Si heterostructure was studied by C–V characteristics for various frequencies from 100 kHz to 3 MHz at room temperature. Fig. 9(a) and (b) display C–V and G–V plots of the Co/giemsa/n-Si heterostructure depending on the frequency, respectively. The plots clearly have inversion (−2 to −0.5 V), depletion (−0.5 to 0 V), and accumulation (0 to 2 V) regions. The capacitance and conductance values did not change in the inversion region, but they exhibited changing profile in the depletion and accumulation region. While the capacitance values decreased, the conductance values increased with increasing frequency. The decreasing capacitance values with increasing frequency is due to that interface states cannot follow ac signal [56]. The increasing conductance values by increasing frequency can be ascribed to existence of the interface states [57].

Authorized licensed use limited to: Bilecik Seyh Edebali Universitesi. Downloaded on December 11,2025 at 08:33:02 UTC from IEEE Xplore. Restrictions apply.

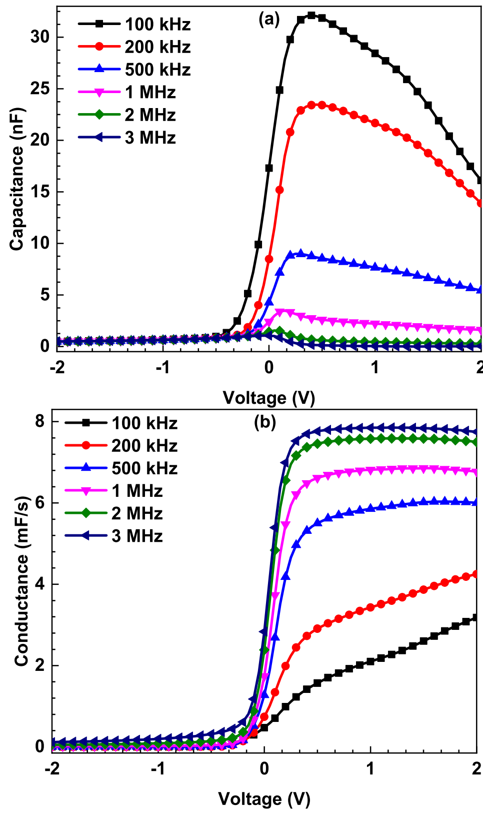

Fig. 9. (a) C–V and (b) G–V plots of the Co/giemsa/n-Si heterostructure for various frequencies.

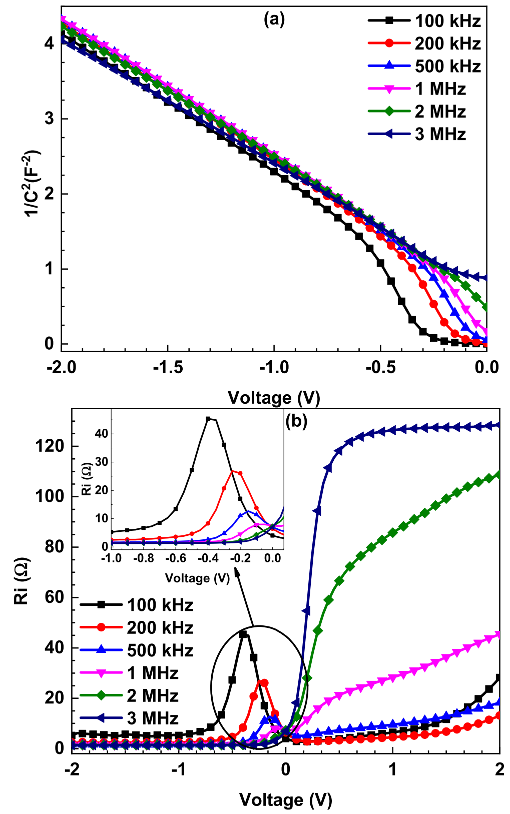

Fig. 10. (a) C^{-2}–V and (b) R_i–V plots of the Co/giemsa/n-Si heterostructure for various frequencies.

The resistance (R_i) of the Co/giemsa/n-Si heterostructure with changing frequency is generally calculated by Nicollian and Brews technique by following formula [58]:

$$R_i = \frac{G_{\text{ma}}}{G_{\text{ma}}^2 + (\omega C_{\text{ma}})^2} \tag{1}$$

where G_{ma} and G_{ma} represent measured conductance and capacitance, respectively. The ω shows angular frequency. The C^{-2}–V plots are employed to calculate various electrical parameters such as interface states (N_{ss}), maximum electric field (E_m), width of depletion region (W_d), carrier concentration of donor atoms (N_d), fermi energy levels (E_F), and barrier height and series resistance (R_s). The calculation of these parameters will be given in the next part.

The C^{-2}–V and R_i–V plots of the Co/giemsa/n-Si heterostructure have been indicated in Fig. 10(a) and (b) for various frequencies, respectively. The C^{-2}–V plots exhibited good linearity from -2 to -0.5 V. The slope and x-intercept of the C^{-2}–V plots provide N_{ss}, E_m, W_d, N_d, and E_F values of the Co/giemsa/n-Si heterostructure. The calculation formulas of these parameters from C^{-2}–V plots can be found everywhere [59]. Among them, the Φ_b is determined by below formula [60]

$$\Phi_b = (V_d + E_F) - \Delta\Phi \tag{2}$$

where V_d and $\Delta\Phi$ indicate diffusion potential which is calculated by $V_d = V_i + \mathrm{k}T/\mathrm{q}$ formula and barrier lowering of image force, respectively. In here, V_i is x-intercept extrapolation of voltage axis for C^{-2}–V plots. The Hill–Coleman technique is used to calculate interface states density (N_{ss}) depending on changing frequency by following formula [61]:

$$N_{\text{ss}} = \frac{2}{qA} \frac{(G_m/\omega)_{\max}}{((G_m/\omega)_{\max}/C_{0x})^2 + (1 - C_m/C_{0x})^2} \tag{3}$$

depending on the conductance (G_m) and capacitance (C_m) values. The C_{ox} is calculated for strong accumulation region by

$$C_{\text{ox}} = C_{\text{ma}} \left[1 + \frac{G_{\text{ma}}^2}{(\omega C_{\text{ma}})^2} \right]. \tag{4}$$

TABLE III
VARIOUS ELECTRICAL PARAMETERS OF THE Co/GIEMSA/n-Si HETEROSTRUCTURE BY INCREASING FREQUENCY

f (kHz)	N_d (10^{17} cm^{-3})	R_s (Ω)	Φ_b (eV)	E_F (eV)	E_m (10^5 v/cm)	W_d (10^{-6} cm)	N_{ss} (10^{11} eV^{-1} cm^{-2})
100	1.01	7.61	0.33	0.1419	0.77	5.34	16.58
200	1.03	4.79	0.44	0.1413	0.99	6.56	10.70
500	1.04	7.22	0.48	0.1412	1.05	6.89	8.18
1000	1.05	13.09	0.50	0.1410	1.08	7.06	4.42
2000	1.08	17.41	0.53	0.1401	1.15	7.19	3.04
3000	1.16	16.93	0.58	0.1383	1.26	7.38	2.45

The values of the electrical parameters have been given in Table III for various frequencies. While the N_{ss} and E_F values decreased, the other parameters increased with increasing frequency. The reason of the decrease at the N_{ss} can be attributed to that the N_{ss} cannot follow ac signal toward high frequencies, and effectiveness of interface states in this region

Authorized licensed use limited to: Bilecik Seyh Edebali Universitesi. Downloaded on December 11,2025 at 08:33:02 UTC from IEEE Xplore. Restrictions apply.

and lower frequencies [62], [63]. The R_i values showed peaks, and their intensity decreased and positions shifted toward accumulation region with increasing frequency in depletion region. However, R_i values increased in accumulation region toward higher frequencies owing to effectiveness of series resistance in this region [64]. Furthermore, R_s values were calculated for accumulation region of C–V and G–V characteristics and tabulated in Table III. Their values increased with increasing frequency.

IV. Conclusion

We used giemsa dye for interlayer film structure between Co and n-type silicon to fabricate Co/giemsa/n-Si heterostructure for extracting temperature- and frequency-dependent electrical behaviors for wide range of temperature and frequencies. While the temperature-dependent I–V was used to determine ideality factor, barrier height, and series resistance changes by changing temperature, the C–V measurements were performed to obtain electrical properties of the Co/giemsa/n-Si heterostructure. The ideality factor valued decreased with increasing temperature, but barrier height values increased linearly. The results highlight the thermal sensor behavior of the Co/giemsa/n-Si heterostructure. Frequency-dependent C–V characteristics were also used to extract various electrical parameters such as maximum electric field, depletion width, barrier height, etc. The results highlight that all electrical parameters are function of the frequency and voltage in terms of C–V characteristics. The Co/giemsa/n-Si heterostructure can be improved for thermal sensing as well as switching applications.

References

[1] S. Wang, J. Yang, T. Toll, J. Yang, W. Zhang, and X. Tang, “Conductivity-limiting bipolar thermal conductivity in semiconductors,” *Sci. Rep.*, vol. 5, no. 1, pp. 1–9, May 2015, doi: 10.1038/srep10136.

[2] Y. Kobayashi et al., “Modulation of electrical potential and conductivity in an atomic-layer semiconductor heterojunction,” *Sci. Rep.*, vol. 6, no. 1, p. 31223, Aug. 2016, doi: 10.1038/srep31223.

[3] R. A. Yotter and D. M. Wilson, “A review of photodetectors for sensing light-emitting reporters in biological systems,” *IEEE Sensors J.*, vol. 3, no. 3, pp. 288–303, Jun. 2003, doi: 10.1109/JSEN.2003.814651.

[4] X. Wang et al., “Recent advances in stretchable field-effect transistors,” *J. Mater. Chem. C*, vol. 9, no. 25, pp. 7796–7828, Jul. 2021, doi: 10.1039/d1tc01082d.

[5] Y. Yan, Y. Zhao, and Y. Liu, “Recent progress in organic field-effect transistor-based integrated circuits,” *J. Polym. Sci.*, vol. 60, no. 3, pp. 311–327, Feb. 2022, doi: 10.1002/pol.20210457.

[6] A. Kocyigit, M. Yilmaz, S. Aydogan, Ü. Incekara, and H. Kacus, “Comparison of n and p type Si-based Schottky photodiode with interlayered Congo red dye,” *Mater. Sci. Semicond. Process.*, vol. 135, Nov. 2021, Art. no. 106045, doi: 10.1016/j.mssp.2021.106045.

[7] M. H. Lee et al., “Two-dimensional materials inserted at the metal/semiconductor interface: Attractive candidates for semiconductor device contacts,” *Nano Lett.*, vol. 18, no. 8, pp. 4878–4884, Aug. 2018, doi: 10.1021/acs.nanolett.8b01509.

[8] A. Kocyigit, M. Yilmaz, Ş. Aydoğan, and Ü. Incekara, “The effect of measurements and layer coating homogeneity of AB on the Al/AB/p-Si devices,” *J. Alloys Compounds*, vol. 790, pp. 388–396, Jun. 2019, doi: 10.1016/j.jallcom.2019.03.179.

[9] M. Yilmaz, A. Kocyigit, B. B. Cirak, H. Kacus, U. Incekara, and S. Aydogan, “The comparison of Co/hematoxylin/n-Si and Co/hematoxylin/p-Si devices as rectifier for a wide range temperature,” *Mater. Sci. Semicond. Process.*, vol. 113, Jul. 2020, Art. no. 105039, doi: 10.1016/j.mssp.2020.105039.

[10] M. Biber, Ş. Aydoğan, Z. Çaldiran, B. Çakmak, T. Karacali, and A. Türüt, “The influence of annealing temperature and time on the efficiency of pentacene: PTCDI organic solar cells,” *Results Phys.*, vol. 7, pp. 3444–3448, 2017, doi: 10.1016/j.rinp.2017.09.014.

[11] M. Gsänger, D. Bialas, L. Huang, M. Stolte, and F. Würthner, “Organic semiconductors based on dyes and color pigments,” *Adv. Mater.*, vol. 28, no. 19, pp. 3615–3645, May 2016, doi: 10.1002/adma.201505440.

[12] M. Yilmaz, A. Kocyigit, S. Aydogan, U. Incekara, Y. Sahin, and H. Kacus, “Influence of illumination intensity on electrical characteristics of Eosin y dye-based hybrid photodiode: Comparative study,” *Appl. Phys. A, Solids Surf.*, vol. 126, no. 10, pp. 1–12, Sep. 2020, doi: 10.1007/s00339-020-03828-4.

[13] E. Erdogan, M. Yilmaz, S. Aydogan, U. Incekara, and H. Kacus, “Schottky barrier engineering in metal/semiconductor structures for high thermal stability,” *Semicond. Sci. Technol.*, vol. 36, no. 7, Jun. 2021, Art. no. 075020, doi: 10.1088/1361-6641/AC01A3.

[14] H. M. Zeyada, H. M. Zidan, A. M. Abdelghany, and I. Abbas, “Structural, optical, and dielectric properties of azure B thin films and impact of thermal annealing,” *J. Electron. Mater.*, vol. 46, no. 7, pp. 4304–4311, Jul. 2017, doi: 10.1007/s11664-017-5381-4.

[15] E. Erdogan, M. Yilmaz, S. Aydogan, U. Incekara, and H. Kacus, “Modification of barrier diode with cationic dye for high power applications,” *Optik*, vol. 232, Apr. 2021, Art. no. 166598, doi: 10.1016/j.ijleo.2021.166598.

[16] Y. S. Ocak, M. Kulakci, T. Kiliçoğlu, R. Turan, and K. Akkiliç, “Current–voltage and capacitance–voltage characteristics of a Sn/methylene blue/p-Si Schottky diode,” *Synth. Met.*, vol. 159, nos. 15–16, pp. 1603–1607, Aug. 2009, doi: 10.1016/j.synthmet.2009.04.024.

[17] B. Bati, “The electrical properties of Al/methylene-blue/n-Si/Au Schottky diodes,” *J. Mod. Phys.*, vol. 7, no. 1, pp. 1–6, 2016, doi: 10.4236/jmp.2016.71001.

[18] I. A.-D.-H. A. Al-Saidi and S. A.-D. Abdulkareem, “Nonlinear optical properties and optical power limiting effect of Giemsa dye,” *Opt. Laser Technol.*, vol. 82, pp. 150–156, Aug. 2016, doi: 10.1016/j.optlastec.2016.03.013.

[19] H. H. Gullu and D. E. Yildiz, “Analysis of forward and reverse biased current–voltage characteristics of Al/Al_2O_3/n-Si Schottky diode with atomic layer deposited Al_2O_3 thin film interlayer,” *J. Mater. Sci., Mater. Electron.*, vol. 30, no. 21, pp. 19383–19393, Nov. 2019, doi: 10.1007/s10854-019-02300-1.

[20] A. Karabulut, İ. Orak, S. Canli, N. Yildirim, and A. Türüt, “Temperature-dependent electrical characteristics of Alq3/p-Si heterojunction,” *Phys. B, Condens. Matter*, vol. 550, pp. 68–74, Dec. 2018, doi: 10.1016/j.physb.2018.08.029.

[21] H. Kacus, Y. Sahin, S. Aydogan, U. Incekara, M. Yilmaz, and M. Biber, “Phenol red based hybrid photodiode for optical detector applications,” *Solid-State Electron.*, vol. 171, Sep. 2020, Art. no. 107864, doi: 10.1016/j.sse.2020.107864.

[22] N. Novkovski and E. Atanassova, “Frequency dependence of C-V characteristics of MOS capacitors containing nanosized high-κ Ta_2O_5 dielectrics,” *Adv. Mater. Sci. Eng.*, vol. 2017, May 2017, Art. no. 9745934, doi: 10.1155/2017/9745934.

[23] S. Mahato, D. Biswas, L. G. Gerling, C. Voz, and J. Puigdollers, “Analysis of temperature dependent current-voltage and capacitance-voltage characteristics of an Au/V_2O_5/n-Si Schottky diode,” *AIP Adv.*, vol. 7, no. 8, Aug. 2017, Art. no. 085313, doi: 10.1063/1.4993553.

[24] A. Kocyigit, I. Orak, Z. Çaldiran, and A. Türüt, “Current–voltage characteristics of Au/ZnO/n-Si device in a wide range temperature,” *J. Mater. Sci., Mater. Electron.*, vol. 28, no. 22, pp. 17177–17184, 2017, doi: 10.1007/s10854-017-7646-3.

[25] N. Chandra, R. Chandra, and V. K. Malik, “Temperature dependent current-voltage characteristics of Pt/MoS_2 Schottky junction,” *MRS Adv.*, vol. 4, nos. 38–39, pp. 2127–2134, Sep. 2019, doi: 10.1557/adv.2019.283.

[26] A. Türüt, “Thermal sensitivity from current-voltage-measurement temperaturecharacteristics in Au/n-GaAs Schottky contacts,” *Turkish J. Phys.*, vol. 45, no. 5, pp. 268–280, Nov. 2021, doi: 10.3906/fiz-2108-15.

[27] I. Josan et al., “Extreme environment temperature sensor based on silicon carbide Schottky diode,” in *Proc. Int. Semiconductor Conf.*, vol. 2, Oct. 2009, pp. 525–528, doi: 10.1109/SMICND.2009.5336658.

[28] H. Kacus, M. Yilmaz, A. Kocyigit, U. Incekara, and S. Aydogan, “Optoelectronic properties of Co/pentacene/Si MIS heterojunction photodiode,” *Phys. B, Condens. Matter*, vol. 597, Nov. 2020, Art. no. 412408, doi: 10.1016/j.physb.2020.412408.

Authorized licensed use limited to: Bilecik Seyh Edebali Universitesi. Downloaded on December 11,2025 at 08:33:02 UTC from IEEE Xplore. Restrictions apply.

[29] Ş. Aydoğan, Ü. Incekara, A. R. Deniz, and A. Türüt, "Extraction of electronic parameters of Schottky diode based on an organic orcein," *Microelectron. Eng.*, vol. 87, no. 12, pp. 2525–2530, Dec. 2010, doi: 10.1016/J.MEE.2010.06.004.

[30] R. Rupp, R. Elpelt, R. Gerlach, R. Schomer, and M. Draghici, "A new SiC diode with significantly reduced threshold voltage," in *Proc. 29th Int. Symp. Power Semiconductor Devices IC's (ISPSD)*, May 2017, pp. 355–358, doi: 10.23919/ISPSD.2017.7988991.

[31] M. Sağlam, B. Güzeldir, A. Türüt, and D. Ekinci, "Role of reduced graphene oxide-gold nanoparticle composites on Au/Au-RGO/p-Si/Al structure depending on sample temperature," *J. Electron. Mater.*, vol. 50, no. 8, pp. 4752–4761, Aug. 2021, doi: 10.1007/s11664-021-09017-0.

[32] Z. Orhan, M. Yilmaz, S. Aydogan, M. Taskin, and U. Incekara, "Improving light-sensing behavior of Cu/n-Si photodiode with human serum albumin: Microelectronic and dielectric characterization," *Optik*, vol. 241, Sep. 2021, Art. no. 167069, doi: 10.1016/j.ijleo.2021.167069.

[33] I. Orak, A. Kocyigit, and A. Türüt, "The surface morphology properties and respond illumination impact of ZnO/n-Si photodiode by prepared atomic layer deposition technique," *J. Alloys Compounds*, vol. 691, pp. 873–879, Jan. 2017, doi: 10.1016/j.jallcom.2016.08.295.

[34] L. D. Rao and V. R. Reddy, "Electrical parameters and series resistance analysis of Au/Y/p-InP/Pt Schottky barrier diode at room temperature," in *Proc. AIP Conf.*, 2016, vol. 1731, no. 1, Art. no. 120020, doi: 10.1063/1.4948092.

[35] F. Yakuphanoglu, "Photovoltaic properties of the organic-inorganic photodiode based on polymer and fullerene blend for optical sensors," *Sens. Actuators A, Phys.*, vol. 141, no. 2, pp. 383–389, Feb. 2008, doi: 10.1016/j.sna.2007.10.023.

[36] S. M. Sze, *Physics of Semiconductor Devices*, vol. 10, 2nd ed. New York, NY, USA: Wiley, 1995.

[37] A. Guzel, S. Duman, N. Yildirim, and A. Türüt, "Electronic transport of an Ni/n-GaAs diode analysed over a wide temperature range," *J. Electron. Mater.*, vol. 45, no. 6, pp. 2808–2814, Jun. 2016, doi: 10.1007/s11664-016-4342-7.

[38] M. A. Mayimele, M. Diale, W. Mtangi, and F. D. Auret, "Temperature-dependent current–voltage characteristics of Pd/ZnO Schottky barrier diodes and the determination of the Richardson constant," *Mater. Sci. Semicond. Process.*, vol. 34, pp. 359–364, Jun. 2015, doi: 10.1016/j.mssp.2015.02.018.

[39] S. K. Cheung and N. W. Cheung, "Extraction of Schottky diode parameters from forward current-voltage characteristics," *Appl. Phys. Lett.*, vol. 49, no. 2, p. 85, Jul. 1986, doi: 10.1063/1.97359.

[40] M. O. Erdal, A. Kocyigit, and M. Yildirim, "Temperature dependent current-voltage characteristics of Al/TiO_2/n-Si and Al/Cu: TiO_2/n-Si devices," *Mater. Sci. Semicond. Process.*, vol. 103, Nov. 2019, Art. no. 104620, doi: 10.1016/j.mssp.2019.104620.

[41] Ş. Karataş, N. Yildirim, and A. Türüt, "Electrical properties and interface state energy distributions of Cr/n-Si Schottky barrier diode," *Superlattices Microstruct.*, vol. 64, pp. 483–494, Dec. 2013, doi: 10.1016/j.spmi.2013.10.015.

[42] H. Norde, "A modified forward I-V plot for Schottky diodes with high series resistance," *J. Appl. Phys.*, vol. 50, no. 7, pp. 5052–5053, Jul. 1979, doi: 10.1063/1.325607.

[43] H. Kacus, M. Yilmaz, U. Incekara, A. Kocyigit, and S. Aydogan, "The photosensitive activity of organic/inorganic hybrid devices based on aniline blue dye: Au nanoparticles (AB@Au NPs)," *Sens. Actuators A, Phys.*, vol. 330, Oct. 2021, Art. no. 112856, doi: 10.1016/J.SNA.2021.112856.

[44] D. A. Aldemir, A. Kökce, and A. F. Özdemir, "Schottky diyot parametrelerini belirlemede kullanilan metotlarin geniş bir sicaklik araliği için kiyaslanmasi," *SAÜ Fen Bilim. Enstitüsü Derg.*, vol. 21, no. 6, p. 1, Dec. 2017, doi: 10.16984/saufenbilder.279996.

[45] S. M. Faraz, M. Willander, and Q. Wahab, "Current transport studies and extraction of series resistance of Pd/ZnO Schottky diode," in *Proc. IEEE 14th Int. Multitopic Conf.*, Dec. 2011, pp. 196–200, doi: 10.1109/INMIC.2011.6151472.

[46] I. Gumus and S. Aydogan, "Thermal sensing capability of metal/composite-semiconductor framework device with the low barrier double Gaussian over wide temperature range," *Sens. Actuators A, Phys.*, vol. 332, Dec. 2021, Art. no. 113117, doi: 10.1016/j.sna.2021.113117.

[47] X. Li, T. Pu, T. Zhang, X. Li, L. Li, and J.-P. Ao, "P-NiO/n-GaN heterostructure diode for temperature sensor application," *IEEE Sensors J.*, vol. 20, no. 1, pp. 62–66, Jan. 2020, doi: 10.1109/JSEN.2019.2939045.

[48] S. Rao, L. Di Benedetto, G. Pangallo, A. Rubino, S. Bellone, and F. G. Della Corte, "85–440 K temperature sensor based on a 4H-SiC Schottky diode," *IEEE Sensors J.*, vol. 16, no. 17, pp. 6537–6542, Sep. 2016, doi: 10.1109/JSEN.2016.2591067.

[49] D. Cordova, P. Toledo, H. Klimach, S. Bampi, and E. Fabris, "0.5 V supply voltage reference based on the MOSFET ZTC condition," in *Proc. 28th Symp. Integr. Circuits Syst. Design*, Aug. 2015, pp. 1–7, doi: 10.1145/2800986.2800988.

[50] X. Li, T. Pu, X. Li, L. Li, and J.-P. Ao, "Correlation between anode area and sensitivity for the TiN/GaN Schottky barrier diode temperature sensor," *IEEE Trans. Electron Devices*, vol. 67, no. 3, pp. 1171–1175, Mar. 2020, doi: 10.1109/TED.2020.2968358.

[51] Y. Wang et al., "Temperature sensing using junctions between mobile ions and mobile electrons," *Proc. Nat. Acad. Sci. USA*, vol. 119, no. 4, Jan. 2022, Art. no. e2117962119, doi: 10.1073/pnas.2117962119.

[52] Q. Guo, F. Lu, Q. Tan, T. Zhou, J. Xiong, and W. Zhang, "Al_2O_3-based a-IGZO Schottky diodes for temperature sensing," *Sensors*, vol. 19, no. 2, p. 224, Jan. 2019, doi: 10.3390/s19020224.

[53] L. Li, J. Chen, X. Gu, X. Li, T. Pu, and J.-P. Ao, "Temperature sensor using thermally stable TiN anode GaN Schottky barrier diode for high power device application," *Superlattice Micro.*, vol. 123, pp. 274–279, Nov. 2018, doi: 10.1016/j.spmi.2018.09.007.

[54] M. S. Gorji and K. Y. Cheong, "Embedded nanoparticles in Schottky and ohmic contacts: A review," *Crit. Rev. Solid State Mater. Sci.*, vol. 40, no. 4, pp. 197–222, Jul. 2015, doi: 10.1080/10408436.2014.940444.

[55] G. Perez et al., "Integrated temperature sensor with diamond Schottky diodes using a thermosensitive parameter," *Diamond Rel. Mater.*, vol. 78, pp. 83–87, Sep. 2017, doi: 10.1016/j.diamond.2017.08.008.

[56] I. Orak, A. Kocyigit, and S. Alindal, "Electrical and dielectric characterization of Au/ZnO/n–Si device depending frequency and voltage," *Chin. Phys. B*, vol. 26, no. 2, 2017, Art. no. 028102, doi: 10.1088/1674-1056/26/2/028102.

[57] M. Yıldırım and A. Kocyigit, "Characterization of Al/In: ZnO/p-Si photodiodes for various In doped level to ZnO interfacial layers," *J. Alloys Compounds*, vol. 768, pp. 1064–1075, Nov. 2018, doi: 10.1016/j.jallcom.2018.07.295.

[58] E. H. Nicollian and J. R. Brews, *MOS (Metal Oxide Semiconductor) Physics and Technology*. Hoboken, NJ, USA: Wiley, 2003.

[59] M. Ulusoy, Ş. Altindal, P. Durmuş, S. Özçelik, and Y. Azizian-Kalandaragh, "Frequency and voltage-dependent electrical parameters, interface traps, and series resistance profile of Au/(NiS:PVP)/n-Si structures," *J. Mater. Sci., Mater. Electron.*, vol. 32, no. 10, pp. 13693–13707, May 2021, doi: 10.1007/s10854-021-05947-x.

[60] İ. Orak and A. Koçyiğit, "The thickness effect of insulator layer between the semiconductor and metal contact on C-V characteristics of Al/Si_3N_4/p-Si device," *Pamukkale Univ. J. Eng. Sci.*, vol. 23, no. 5, pp. 536–542, 2017, doi: 10.5505/pajes.2016.23911.

[61] W. A. Hill and C. C. Coleman, "A single-frequency approximation for interface-state density determination," *Solid-State Electron.*, vol. 23, pp. 987–993, Sep. 1980, doi: 10.1016/0038-1101(80)90064-7.

[62] Ç. Bilkan, Ş. Altindal, and Y. Azizian-Kalandaragh, "Investigation of frequency and voltage dependence surface states and series resistance profiles using admittance measurements in Al/p-Si with Co_3O_4-PVA interlayer structures," *Phys. B, Condens. Matter*, vol. 515, pp. 28–33, Jun. 2017, doi: 10.1016/J.PHYSB.2017.04.002.

[63] A. Nikravan, Y. Badali, Ş. Altindal, İ. Uslu, and İ. Orak, "On the frequency and voltage-dependent profiles of the surface states and series resistance of Au/ZnO/n-Si structures in a wide range of frequency and voltage," *J. Electron. Mater.*, vol. 46, no. 10, pp. 5728–5736, Oct. 2017, doi: 10.1007/s11664-017-5613-7.

[64] I. Orak, A. Kocyigit, İ. Karteri, and S. Uruş, "Frequency-dependent electrical characterization of GO-SiO_2 composites in a Schottky device," *J. Electron. Mater.*, vol. 47, no. 11, pp. 6691–6700, Nov. 2018, doi: 10.1007/s11664-018-6571-4.

Authorized licensed use limited to: Bilecik Seyh Edebali Universitesi. Downloaded on December 11,2025 at 08:33:02 UTC from IEEE Xplore. Restrictions apply.